Supporting Information

Iron-Copper Bimetallic Nanocomposite Reinforced Dressing Materials for Infection Control and Healing of Diabetic Wound

Madhumita Das,[a,b] *Upashi Goswami,*[a] *Raghuram Kandimalla,*[c] *Sanjeeb Kalita,*[c] *Siddhartha Sankar Ghosh,*[*a,d] *and Arun Chattopadhyay*[*a,e]

[a]Centre for Nanotechnology, Indian Institute of Technology Guwahati, Guwahati 781039

[b]Guwahati Neurological Research Centre Medical Lab, North Guwahati 781031

[c]Institute of Advance Study of Science and Technology, Guwahati 781035

[d]Department of Biosciences and Bioengineering, Indian Institute of Technology Guwahati, Guwahati 781039

[e]Department of Chemistry, Indian Institute of Technology Guwahati, Guwahati 781039

***Email: arun@iitg.ac.in; sghosh@iitg.ac.in**

*Materials:*All reagents were used as received without further purification.The sources for the bandage materials were extra pure hydrate ferrous chloride (LobaChemie), ferric chloride anhydrous, copper II sulphate pentahydrate ($CuSO_4.5H_2O$), 25% ammonia solution and 80% hydrazine hydrate (Merck). Iodine was purchased from Sigma Aldrich chemical Pvt.Ltd. Kolkata, India. Milli-Q grade (resistivity 18.2 MΩcm-1) water was used in all experiments. Different species of microorganisms (Methicillin resistant *S.aureus*, *E.coli and C.albicans)* used in the experiments were isolated from various patients' samples collected from patients attending Guwahati Neurological Research Center (GNRC) Medical Outdoor Clinic or admitted there for treatment after taking written consent from them. The media used for growth of these microorganisms were cysteine lactose electrolyte deficient agar (CLED), nutrient agar, Muller Hinton agar (MHA) and MHA with 2% glucose and 0.5 mg/L methylene blue dye for fungus, purchased from Himedia, Mumbai, India.

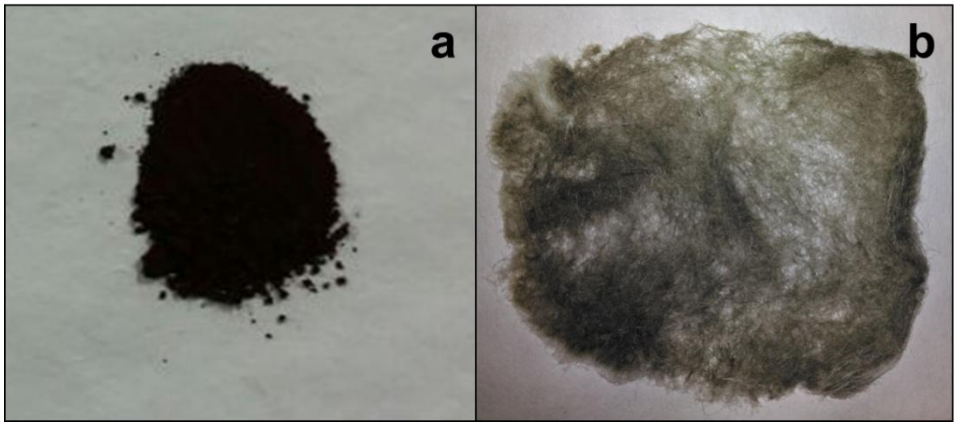

Figure S1. Photographs of (a) the dressing material in powder form (Fe-Cu-nanocomposite) and (b) the dressing bed prepared in cotton swab by impregnating bimetallic Fe-Cu-nanocomposite in it.

Transmission Electron Microscopy (TEM): The presence of nanoparticles in Fe-Cu-nanocomposite powder was confirmed by TEM (Figure S2a). Distinct SAED patterns (Figure S2b) with lattice spacing of 0.108, 0.18 and 0.2 nm were indexed to 311, 200 and 111 planes, respectively, of Cu in cubic (fcc) structures. Whereas the values of 0.128 (311) for Cu_2O and 0.127 (104), 197 (112) and 0.205 (012) reflections were for CuO.[1,2] Again the diffraction with prominent ring and interplanar spacing value of 0.171 nm was indexed to 511 planes of Fe_3O_4[3], which confirmed the presence of iron oxide and copper oxide nanoparticles along with Cu in

zero oxidation state. Similarly, the TEM of Fe-Cu-nanocomposite impregnated cotton swabs were also conducted (Figure S2d), which validated the synthesis of spherical Fe-Cu containing nanoparticles on cotton swab. At the same time, the diffraction patterns in SAED (Figure S2e), showed prominent rings with interplanar spacing value of 0.128 and 0.211 nm corresponding to 311 and 200 planes for Cu_2O. The values of 0.107, 0.12, 0.19 nm corresponding to 311, 220 and 111 planes for Cu in cubic (fcc) structures and diffraction at 0.126, 0.157, 0.196, 0.208 nm corresponding to 104, 220, 112 and 012 planes were for CuO.[1,2] Again, the lattice spacing of 0.157 and 0.171 were indexed to 440 and 511 planes of Fe_3O_4[3] and hence confirmed the presence of both Fe and Cu oxide nanoparticles along with Cu in zero oxidation state.

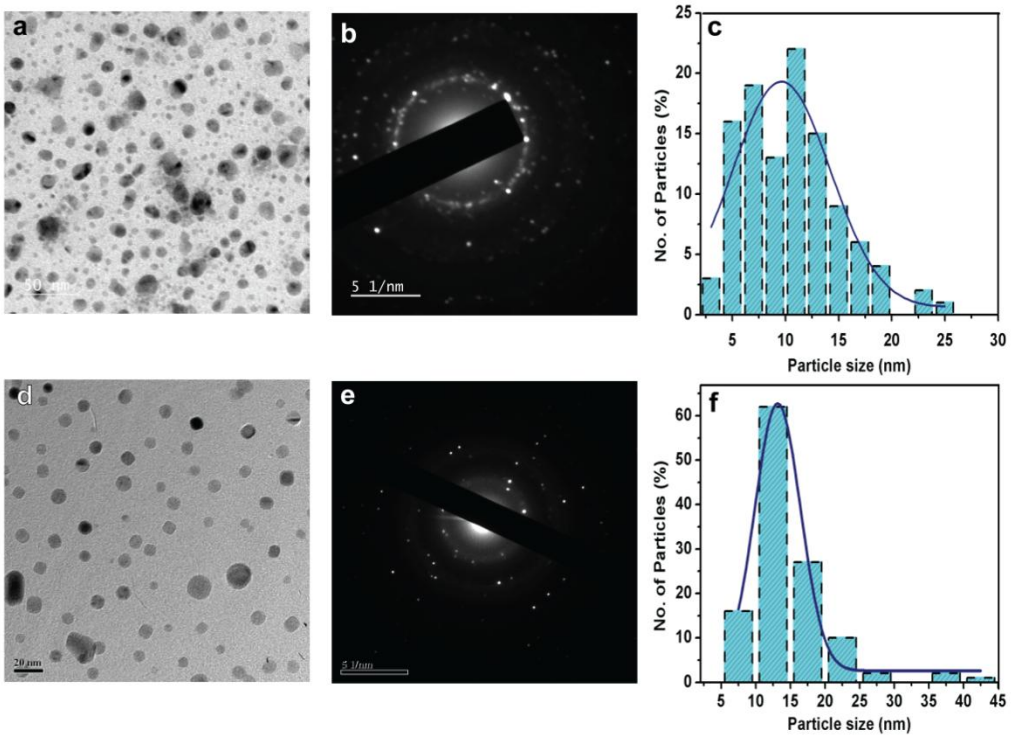

Figure S2. (a) TEM image, (b) SAED image and (c) histogram showing particle size distribution of bimetallic Fe-Cu-nanocomposite powder. (d) TEM image, (e) SAED image and (f) histogram showing particle size distribution of Fe-Cu-nanocomposite prepared *in situ* on cotton swab.

***Powder X-Ray Diffraction Study (XRD)*:** Subsequently, powder XRD pursued on both the dressing materials also established the existence of iron oxide and copper oxide NPs in them. The XRD patterns of Fe-Cu-nanocomposite powder (Figure S3a) showed diffraction at 2θ values

of 24.1^0(012), 33.3^0(104), 35.6^0(110), 40.2^0(113), 43.2^0(202), 49.3^0(024), 54.2^0(116), 57.6^0(018), 62.8^0(214), 64.0^0 (300) and 72.0^0(119), which suggested the formation of Fe_2O_3. The presence of Fe_3O_4 NPs were confirmed by the peaks obtained at 17.9^0 (111), 21.3^0 (020), 30.5^0 (220), 35.6^0 (311), 43.2^0 (400), 54.2^0 (422), 57.6^0 (511) and 62.8^0 (440).[4-10] Existence of cupric oxide (CuO) and cuprous oxide (Cu_2O) NPs were validated with peaks at 2θ value of 33.3^0 (-110), 35.6^0 (002/11-1), 46.3^0 (-112), 49.3^0 (-202), 57.6^0 (002/202), 61.3^0 (-113), 68.0^0 (113), 75.4^0 (-222) and 36.5^0 (111), 61.3^0 (220), 72.0^0 (311), 75.4^0 (222), respectively.[11,12] Plain cotton swab (Figure S3b) showed major diffraction at 15.1^0 (101), 16.9^0 (10$\underline{1}$), 23.1^0 (002) and 34.8^0 (040) due to cellulose I.[13] Similarly, powder XRD was also conducted on Fe-Cu-nanocomposite impregnated cotton swab (Figure S3c) where diffractions at 2θ values of 33.6^0 (104), 41.5^0 (113), 43.7^0 (202), 49.8^0 (024), 54.6^0 (116), 57.7^0 (018), 63.0^0 (214), 64.3^0 (300) and 72.4^0 (119) indicated the formation of Fe_2O_3 NPs whereas peaks at 30.8^0 (220), 43.7^0 (400), 54.6^0 (422), 57.7^0 (511), and 63.0^0 (440) were for Fe_3O_4.[4-10] The peaks at 2θ values of 33.6^0 (-110), 49.8^0 (-202), 53.8^0 (020/20-2), 57.7^0 (002/202), 61.5^0 (-113) and 75.5^0 (-222) suggested the existence of CuO NPs whereas formation of Cu_2O was corroborated by peaks at 2θ values of 36.0^0 (111), 61.5^0 (220), 72.4^0 (311) and 75.5^0 (222).[11-12] Diffraction from cellulose I of cotton swab was observed at 16.6^0 (101) and 23.1^0 (002).[13] The values in the parentheses represent the planes of diffractions as observed in XRD.

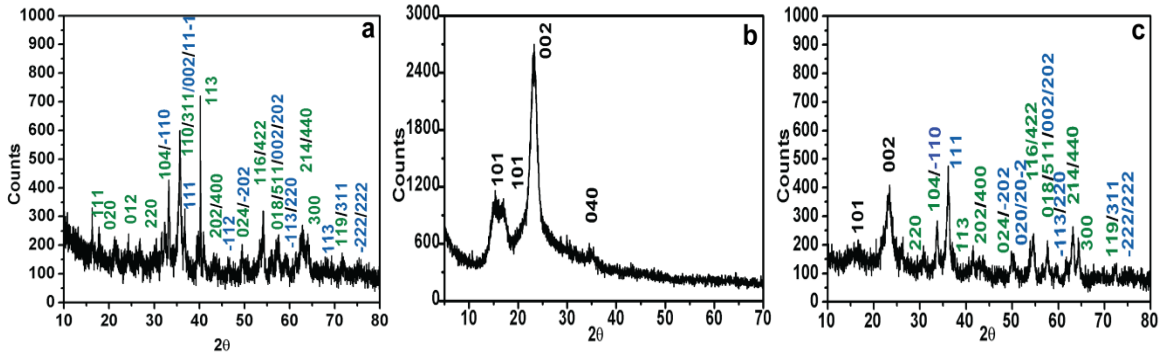

Figure S3. XRD patterns of (a) Fe-Cu-nanocomposite powder, (b) plain cotton and (c) Fe-Cu-nanocomposite embedded cotton swab, where peaks marked in black indicate diffractions due to cellulose, green for Fe_2O_3/Fe_3O_4 and blue is for Cu_2O/CuO.

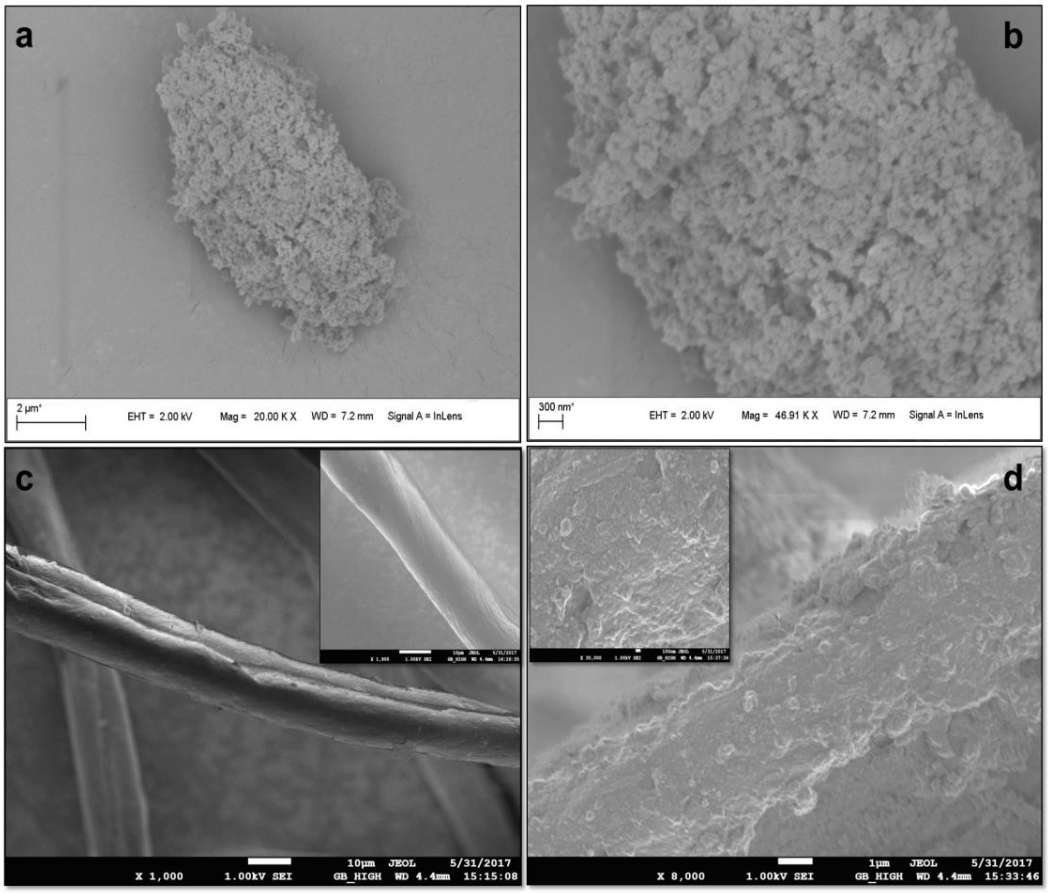

Figure S4. FESEM image of (a) Fe-Cu-nanocomposite powder and (b) magnified image of the same. FESEM image of (c) cotton (inset is the magnified image) and (d) that of Fe-Cu-nanocomposite impregnated cotton swab. Insets represent magnified images of those in (c) and (d), respectively.

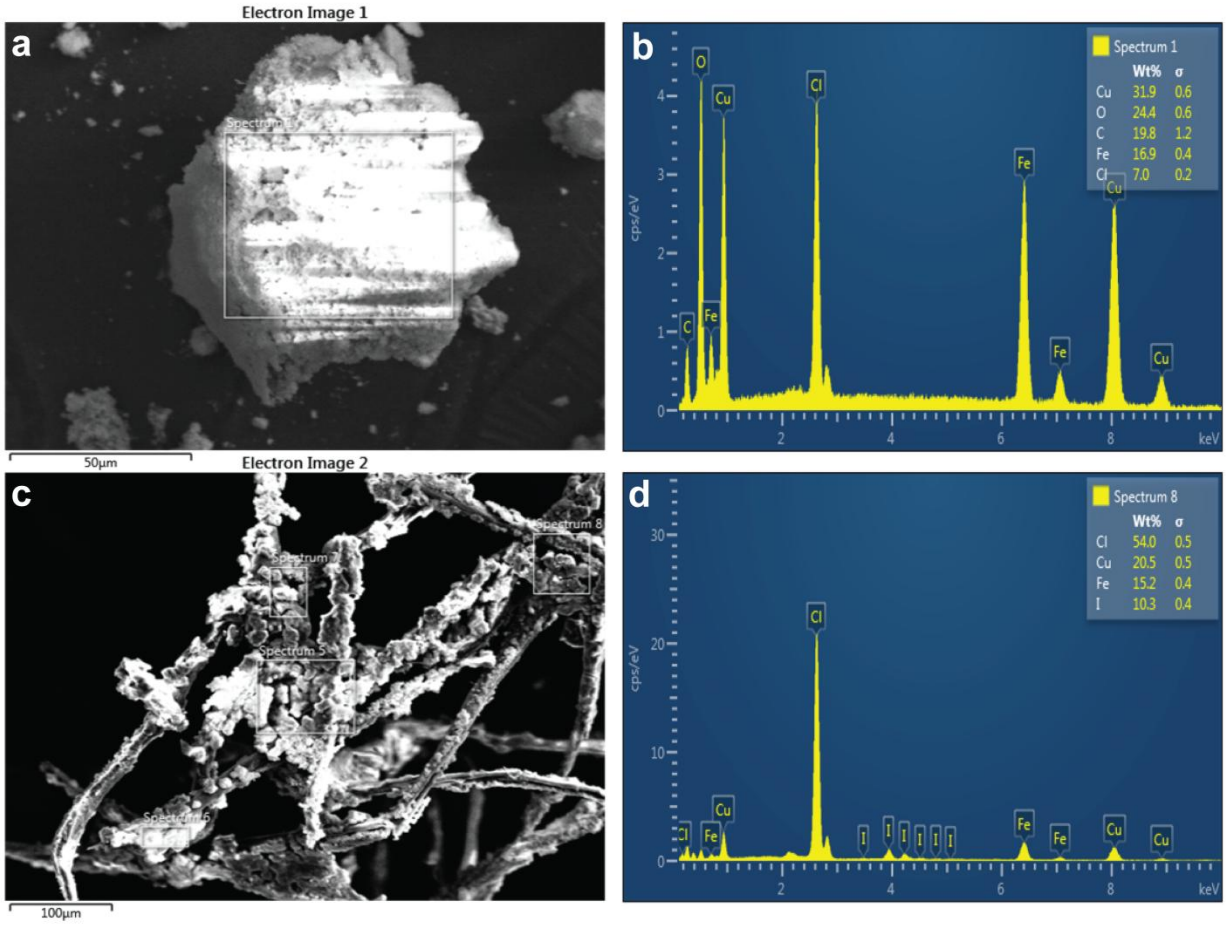

Figure S5. (a) FESEM micrograph of Fe-Cu-nanocomposite powder and (b) EDX result for a specific spot on the nanocomposite. (c) FESEM micrograph of Fe-Cu-nanocomposite impregnated cotton swab and (d) EDX result for a specific spot on the nanocomposite impregnated cotton.

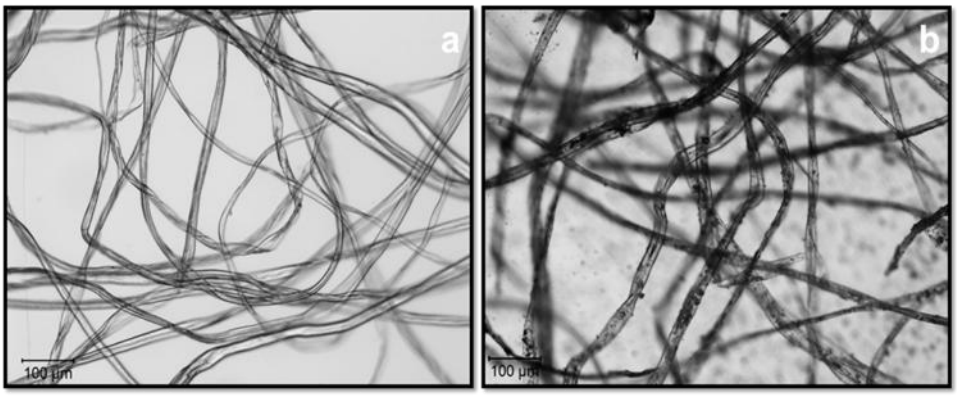

Figure S6. Bright field image of (a) cotton and (b) nanocomposite impregnated cotton swab recorded using the confocal microscope.

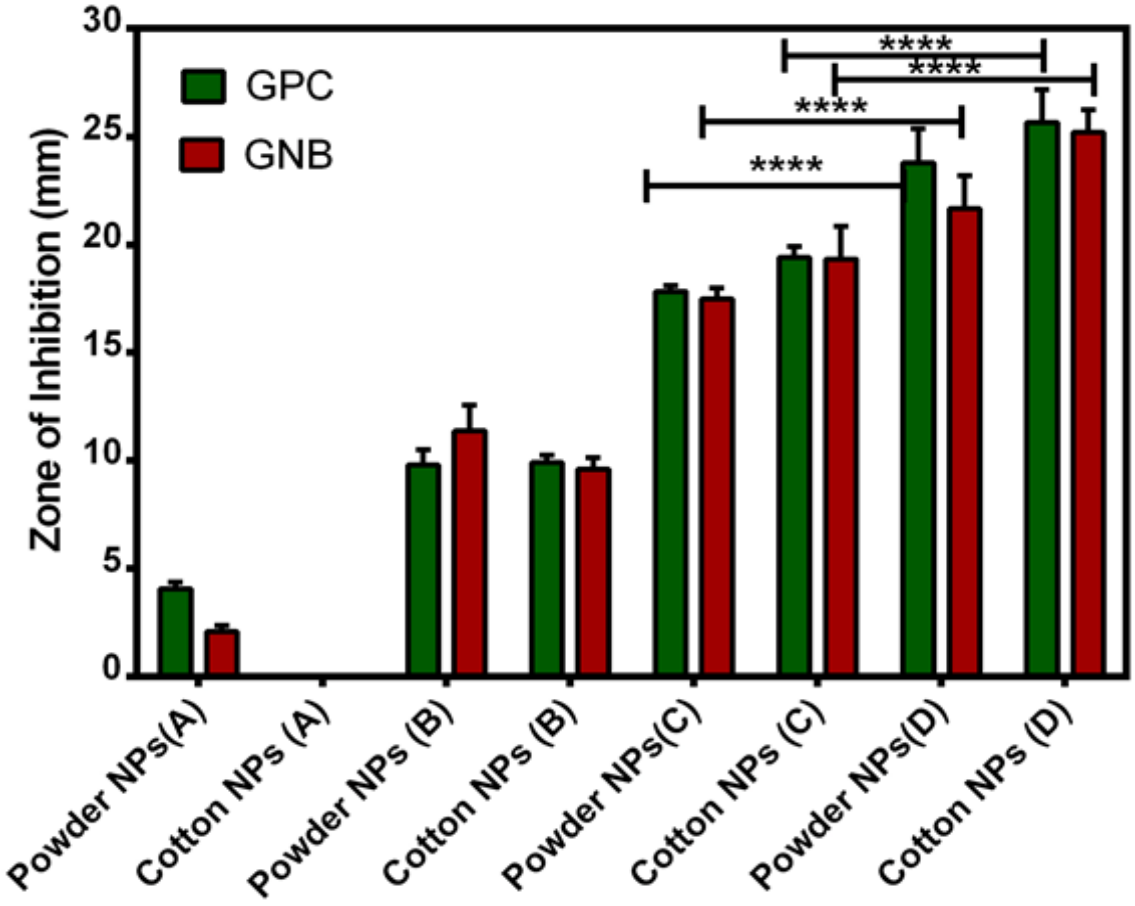

Figure S7. Comparison of the antimicrobial activities (in terms of zone of inhibition) of the (different) prepared materials against methicillin resistant *S. aureus* (GPC) and *E. coli* (GNB). Here powder NPs (A) represents FeNPs in powder form, cotton NPs (A) represents FeNPs impregnated cotton, powder NPs (B) represents CuNPs in powder form, cotton NPs (B) represents CuNPs impregnated cotton, powder NPs (C) represents Fe-Cu-nanocomposite in powder form prepared without iodine, cotton NPs (C) represents Fe-Cu-nanocomposite impregnated cotton prepared without iodine, powder NPs (D) represents powder Fe-Cu-nanocomposite stabilized with iodine and cotton NPs (D) represents Fe-Cu-nanocomposite impregnated cotton stabilized with iodine.

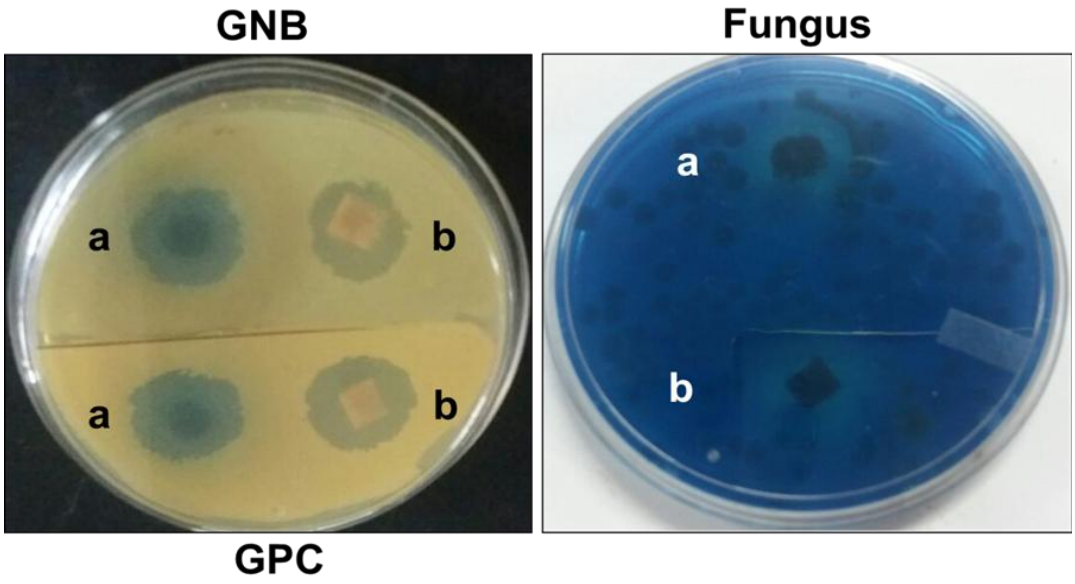

Figure S8. Plate with growth of both GPC (*S.aureus*)-lower left, GNB (*E.coli*)-upper left and fungus (*C.albicans*)-right, showing clear zone of inhibition around (a) powder NPs and (b) cotton NPs tested one month after preparation.

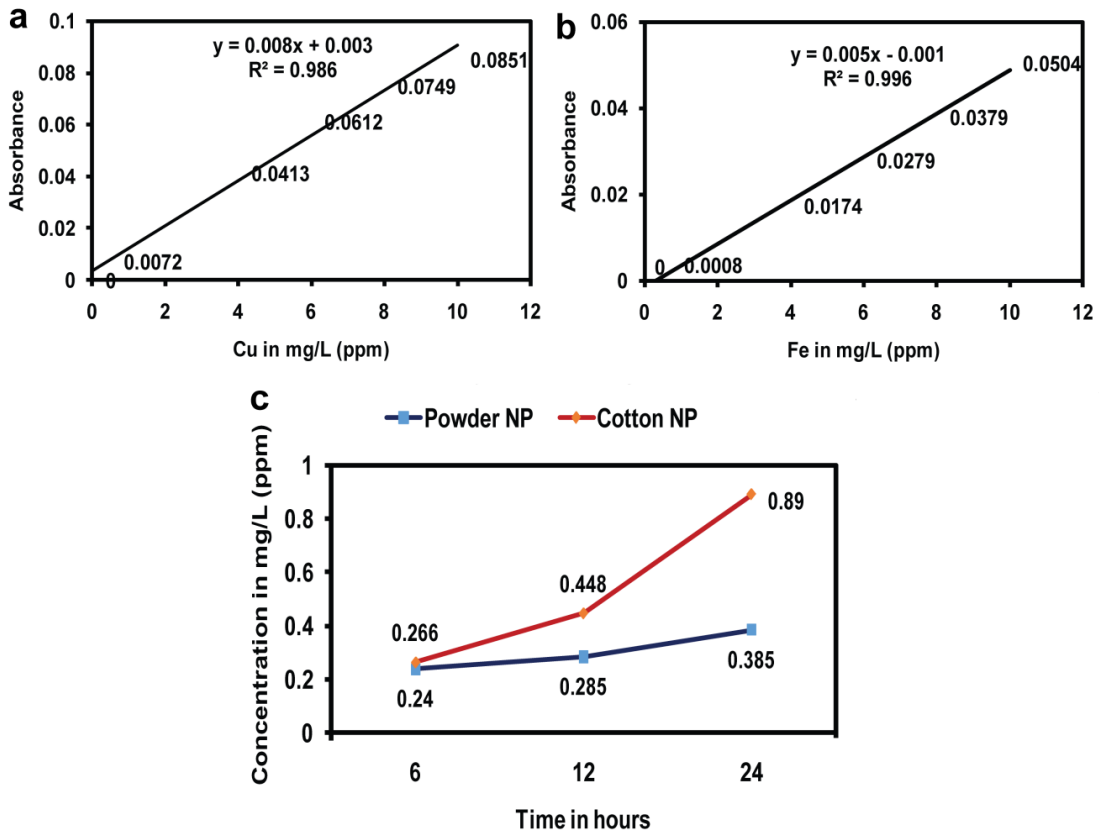

Figure S9. Results of atomic absorption spectroscopy where part (a) represents standard graph of copper, (b) represents standard graph of iron, and part (c) represents the results of the release study of copper tested in PBS buffer. The blue line represents the concentration of copper that is released at 6, 12 and 24 h from the powder form of dressing material and the red line represents the concentration of copper released from the cotton embedded with the nanocomposite.

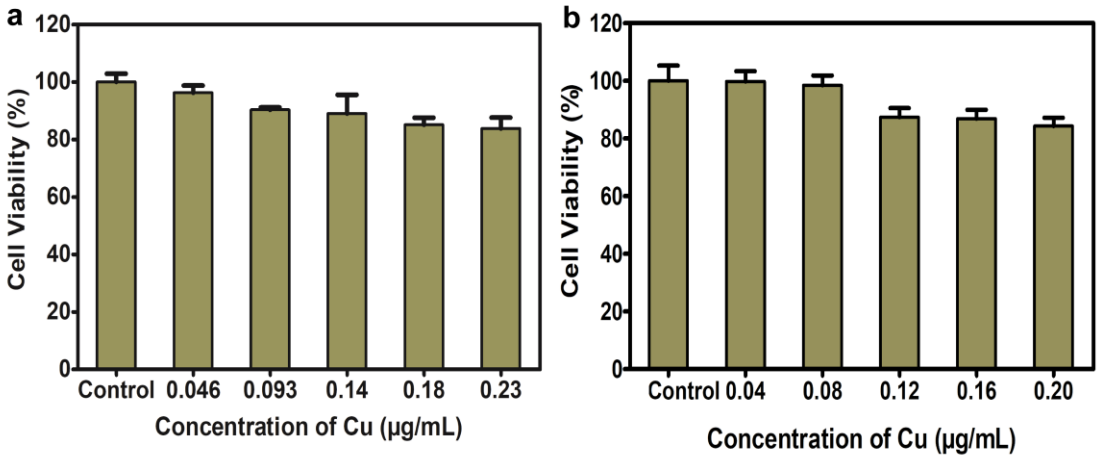

Figure S10. Results of cytotoxicity based on MTT assay after 48 h of treatment with varying concentrations of powder form of dressing materials (a) and cotton embedded with nanocomposite (b) in HEK 293 cells. The experiments were carried out in triplicate and are represented as the mean ± SD.

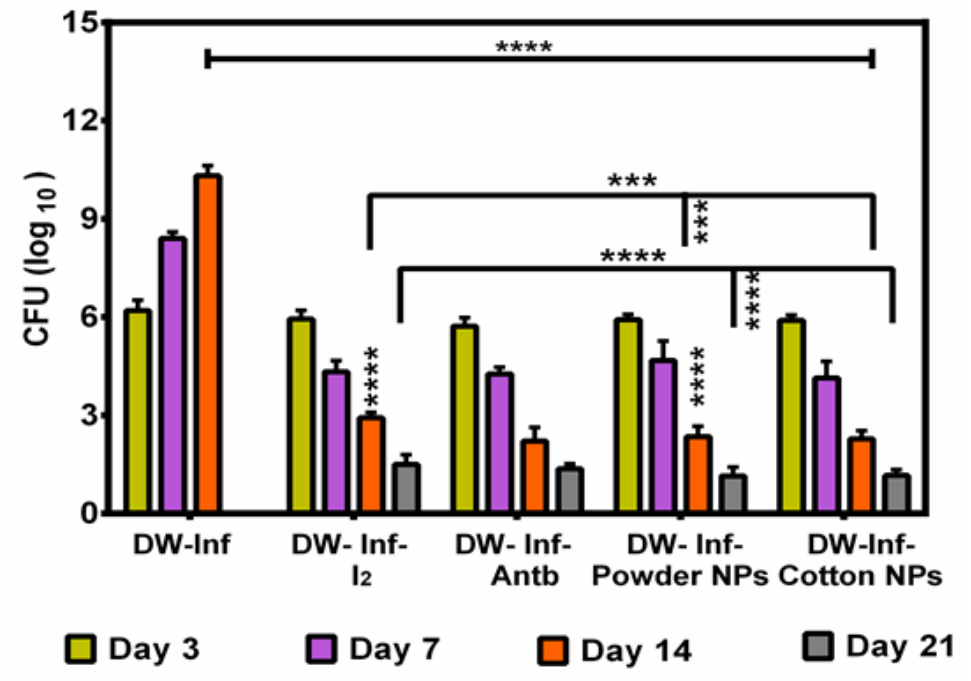

Figure S11. Number of colony forming bacteria at the wound site of different infected groups on day 3, 7, 14 and 21 where, DW-Inf represents rat with infected diabetic wound, DW-Inf-I_2- rat with infected diabetic wound treated with iodine, DW-Inf-Antb- rat with infected diabetic wound treated with conventional topical antibiotic, DW-Inf-powder NPs- rat with infected diabetic wound treated with nanocomposites powder and DW-Inf-Cotton NPs- rat with infected diabetic wound treated with nanocomposites impregnated cotton.

Additional Figure:

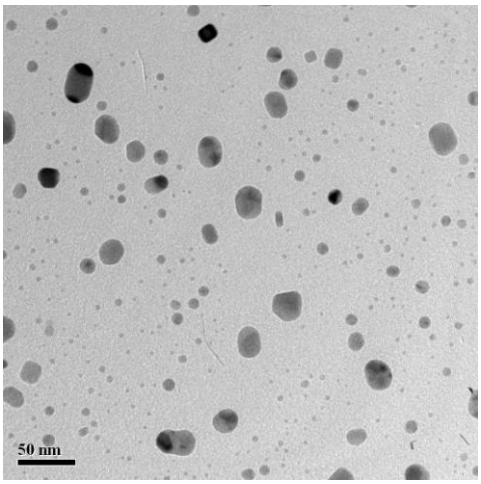

Figure S12. TEM image of the nanocmposite powder conducted one month after preparation showing distinct round to oval nanoparticles without any evidence of agglomeration.

REFERENCES

1. Gholinejad, M.; Saadati, F.; Shaybanizadeh, S.; Pullithadathil, B. Copper Nanoparticles Supported on Starch Micro Particles as a Degradable Heterogeneous Catalyst for Three-Component Coupling Synthesis of Propargylamines. *RSC Adv.***2016**, *6* (6), 4983–4991. https://doi.org/10.1039/c5ra22292c.

2. Kozak, D. S.; Sergiienko, R. A.; Shibata, E.; Iizuka, A.; Nakamura, T. Non-Electrolytic Synthesis of Copper Oxide/Carbon Nanocomposite by Surface Plasma in Super-Dehydrated Ethanol. *Sci. Rep.***2016**, *6*, 1–9. https://doi.org/10.1038/srep21178.

3. Knappett, B. R.; Abdulkin, P.; Ringe, E.; Jefferson, D. A.; Lozano-Perez, S.; Rojas, T. C.; Fernández, A.; Wheatley, A. E. H. Characterisation of Co@Fe3O4 Core@shell Nanoparticles Using Advanced Electron Microscopy. *Nanoscale*, **2013**, *5* (13), 5765. https://doi.org/10.1039/c3nr33789h.

4. Blanco-Andujar, C.; Ortega, D.; Pankhurst, Q. A.; Thanh, N. T. K. Elucidating the Morphological and Structural Evolution of Iron Oxide Nanoparticles Formed by Sodium Carbonate in Aqueous Medium. *J. Mater. Chem.* **2012**, *22* (25), 12498. https://doi.org/10.1039/c2jm31295f.

5. Morris, M. C.; McMurdie, H. F.; Evans, E. H.; Paretzkin, B.; Parker, H. S.; Panagiotopoulos, N. C.; Hubbard, C. R. Standard X-ray Diffraction Powder Patterns; U.S. Department of Commerce, NBS:Washington, D.C., **1981**; Vol. 37.

6. Salem, N. M.; Awwad, A. M. A Novel Approach for Synthesis Magnetite Nanoparticles at Ambient Temperature. *Nanosci. Nanotechnol.* **2013**, *3* (3), 35–39. https://doi.org/10.5923/j.nn.20130303.01.

7. Sukumar, U. K.; Gopinath, P. Field-Actuated Antineoplastic Potential of Smart and Versatile PEO-BPEI Electrospun Scaffold by Multi-Staged Targeted Co-Delivery of Magnetite Nanoparticles and Niclosamide-BPEI Complexes. *RSC Adv.* **2016**, *6* (52), 46186–46201. https://doi.org/10.1039/c6ra05006a.

8. Zhuang, L.; Zhang, W.; Zhao, Y.; Shen, H.; Lin, H.; Liang, J. Preparation and

Characterization of Fe_3O_4 Particles with Novel Nanosheets Morphology and Magnetochromatic Property by a Modified Solvothermal Method. *Sci. Rep.* **2015**, *5*, 1–6. https://doi.org/10.1038/srep09320.

9. Wei, H.; Hu, D.; Su, J.; Li, K. Intensification of Levofloxacin Sono-Degradation in a US/H_2O_2 System with Fe_3O_4 Magnetic Nanoparticles. *Chinese J. Chem. Eng.* **2015**, *23* (1), 296–302. https://doi.org/10.1016/j.cjche.2014.11.011.

10. Yu, X.; Cheng, G.; Zheng, S. Y. Synthesis of Self-Assembled Multifunctional Nanocomposite Catalysts with Highly Stabilized Reactivity and Magnetic Recyclability. *Sci. Rep.* **2016**, *6* (May), 1–11. https://doi.org/10.1038/srep25459.

11. Jia, B.; Qin, M.; Zhang, Z.; Cao, Z.; Wu, H.; Chen, P.; Zhang, L.; Lu, X.; Qu, X. The Formation of CuO Porous Mesocrystal Ellipsoids via Tuning the Oriented Attachment Mechanism. *CrystEngComm*, **2016**, *18* (8), 1376–1383. https://doi.org/10.1039/c5ce02249e.

12. Meghana, S.; Kabra, P.; Chakraborty, S.; Padmavathy, N. Understanding the Pathway of Antibacterial Activity of Copper Oxide Nanoparticles. *RSC Adv.* **2015**, *5* (16), 12293–12299. https://doi.org/10.1039/c4ra12163e.

13. Liu, Y.; Thibodeaux, D.; Gamble, G.; Bauer, P.; VanDerveer, D. Comparative Investigation of Fourier Transform Infrared (FT-IR) Spectroscopy and X-Ray Diffraction (XRD) in the Determination of Cotton Fiber Crystallinity. *Appl. Spectrosc.* **2012**, *66* (8), 983–986. https://doi.org/10.1366/12-06611.